J Mater Sci (2007) 42:1833–1837
DOI 10.1007/s10853-006-0821-1

Structural and catalytic properties of $Zn_{1-x}Cu_xFe_2O_4$ nanoparticles

M. Banerjee · N. Verma · R. Prasad

Received: 17 February 2006 / Accepted: 18 August 2006 / Published online: 16 December 2006

Abstract A series of zinc copper mixed ferrites having general formula $Zn_{1-x}Cu_xFe_2O_4$ (x = 0.0, 0.25,0.50,0.75,1.0) have been synthesized by co-precipitation method. The average particle sizes of these ferrites as determined from XRD data using Scherer's relation have been found to range from 10.45 to 18.39 nm. The samples have been characterized by XRD, Mössbauer spectroscopy, B.E.T.surface area and acidity measurements. These ferrites have been tested for their catalytic activity in alkylation of pyridine by methanol. The conversion of pyridine as well as yield to 3-methyl pyridine is found to be lowest in case of $ZnFe_2O_4$ which increases as the copper content is increased and is maximum for $CuFe_2O_4$. The results on the acidity measurements on these ferrites as well as structural properties support these results. $CuFe_2O_4$ is found to be highly selective for 3-methyl-pyridine.

M. Banerjee (✉) · N. Verma
School of Physics, Devi Ahilya University, Vigyan Bhawan, Takshashila Parisar, Khandwa Road, Indore 452017, India
e-mail: mandira_bm@rediffmail.com

R. Prasad
School of Chemical Sciences, Devi Ahilya University, Vigyan Bhawan, Takshashila Parisar, Khandwa Road, Indore 452017, India

Present Address:
N. Verma
Dipartminta di Fisica Generale, Universitá di Torino, Torino, Italy

Introduction

Ferrites are magnetic materials, which exhibit high electrical resistivity, low eddy currents, and low dielectric loss and are extensively used in microwave devices, computer memories and magnetic recordings. The attractive feature of ferrites is that their properties can be controlled in a broad measure to suit the particular application.

The formula for ferrospinel is given by $M^{2+}[Fe_2^{3+}]\ O_4^{2-}$. The metal ion in square bracket occupies octahedral position or B site and the metal ions outside the bracket occupy tetrahedral site or A site. Depending upon the position of metals in the tetrahedral and octahedral sites, the ferrospinels can be normal $M^{2+}[Fe_2^{3+}]\ O_4^{2-}$, inverse $Fe^{3+}\ [M^{2+}\ Fe^{3+}]O_4^{2-}$, Or mixed in which the divalent cations are distributed between both the sites. M^{2+} represents divalent ions such as Mn^{2+}, Co^{2+}, Cu^{2+}, Zn^{2+} etc. Ferrite spinels may also contain mixture of two divalent metal ions such as (Mn, Zn) Fe_2O_4 in which Mn^{2+} and Zn^{2+} ratio may be varied. These are called mixed ferrites. Mixed zinc ferrites are technically important and have been studied by several workers [1–4]. This cation distribution of mixed ferrites significantly affects the acido-basic and surface properties of ferrospinels making them catalytically active.

Because of their small particle size, high surface to volume ratio and large number of coordination sites nanoparticles are capable of enhancing the rate of chemical reactions and are increasingly gaining popularity as reactive nanoparticles(RNP). Previous studies of ferrospinels have shown that nano size ferrites of Zinc–Nickel, Zinc–Manganese are excellent catalysts for alkylation of aromatics [5–10]. Alkylated aromatics

such as alkylated aniline, pyridine and phenol find commercial application as raw materials for fine chemicals and bulk drugs. To the best of our knowledge, there is no report on the alkylation of pyridine using nanocrystalline Zn–Cu ferrite as catalyst. The present problem of structural and catalytic properties of $Zn_{1-x}Cu_x$ Fe_2O_4 was therefore undertaken with a view to (1) synthesize a series of nanocrystalline Zn–Cu ferrite (2) to confirm the phase purity and compute partcle size using XRD techniques (3) to predict the distribution of cations and nature of Fe–O bond from Mössbauer study (4) to evaluate the surface area and acidity of samples (5) to evaluate their catalytic performance for alkylation of Pyridine and (6) to find correlation of physico-chemical properties and catalytic activity.

Experimental

Ferrite samples were prepared by co-precipitation method. In this method required amount of metal chlorides were dissolved in excess of water and hydroxides precipitated at a pH of 8 under vigorous stirring. The precipitate was washed free of chlorides, dried and calcined at 773 K for 5 h. The details are described elsewhere [9].

X-ray diffraction patterns were obtained with a Siemens D500 x-ray powder diffractometer using Cu Kα radiation ($\lambda = 1.54$ Å) and graphite crystal monochromator. FTIR spectra were recorded using DIGILAB, SCIMITAR series spectrometer, version—3.3.1.014.

Room temperature Mössbauer spectra were recorded with a conventional constant acceleration spectrometer in the velocity range ± 10 mm s^{-1} in transmission mode using ^{57}Co in rhodium matrix as source. The velocity calibration was performed with laser beam using an iron foil as reference. All Mössbauer parameters are relative to metallic iron.

Acidity measurements were made by ammonia desorption method. In this method acidity of the catalyst is determined using ammonia as adsorbate. 5 g of the catalyst was packed in a Pyrex tube down flow reactor and heated to 673 K under nitrogen gas flow rate of 0.5 cm^3 s^{-1} for 3 h. The reactor was then cooled to 298 K and adsorption conducted at this temperature by exposing the sample to ammonia for 2 h. Physically adsorbed ammonia was removed by purging the sample with a nitrogen gas flow rate of 0.5 cm^3 s^{-1} at 353 K for 1 h. The acid strength distribution was obtained by raising the catalyst temperature from 353 to 773 K in a flow of nitrogen gas of 0.5 cm^3 s^{-1} and absorbing the ammonia evolved in 0.1 N HCl. Quantitative estimation was made by titrating the untreated acid with standard 0.1 M NaOH solution in different temperature ranges using phenolphthalein as indicator.

The methylation of pyridine was carried out in a fixed bed down-flow Pyrex glass tubular reactor (0.45 m in length and 0.025 m internal diameter) at atmospheric pressure. The upper half worked as a preheater and the lower part worked as a reactor, where the catalyst was packed between two plugs of Pyrex glass wool. The catalyst was activated at 773 K by passing air and then cooled down to desired temperature by current of nitrogen. The mixture of pyridine and methanol was fed by a 10 cm^3 pressure-equalizing funnel. The liquid products were condensed with help of a cold water condenser and cold trap and were analyzed with Shimadzu 14B gas chromatograph using Se-30 column and FID detector.

Results and Discussion

The powder diffraction patterns of zinc-copper ferrites are reproduced in Fig. 1. The spinel peaks corresponding to [220], [311], [222], [400]. [422] , [511], [440] planes can be seen clearly confirming the formation of single phase spinel oxides. The broadening of the peaks can be attributed to the small size of the particles of polycrystalline powder.

$ZnFe_2O_4$ is a cubic spinel and the peak positions in Fig. 1 match well with the reported values [11, 12]. $CuFe_2O_4$ can have tetragonal as well as cubic lattice. While slow cooling leads to stable tetragonal structure [13], nanoparticles prepared by co-precipitation method crystallize into metastable cubic structure. The XRD pattern of our samples prepared by co-precipitation method match with those reported by others [14, 15] confirming the cubic structure and the formation of tetragonal form is ruled out.

The XRD pattern of intermediate compounds also match with that of $CuFe_2O_4$ confirming cubic spinel formation. Evans and Hafner [13] have also assigned cubic structure to bulk $Zn_{o.5}$ $Cu_{0.5}$ Fe_2O_4. The particle sizes were calculated using Scherer formula [16] and are listed in Table 1. The partcle size was found to vary in the range 10.45–18.39 nm.

The variation of lattice parameter a_0 as a function of compositional parameter x is shown in Table 1. A continuous decrease in the lattice parameter with increasing Cu content suggests formation of solid solution between $ZnFe_2O_4$ and $CuFe_2O_4$. The observed decrease in a_0 with increasing content of

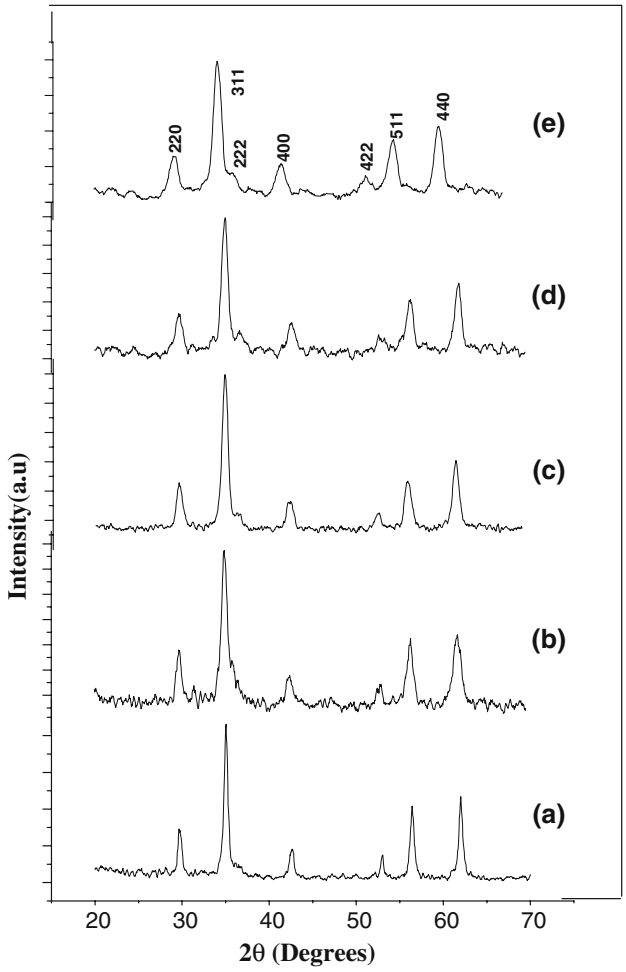

Fig. 1 XRD patterns of of $Zn_{1-x}Cu_xFe_2O_4$ (**a**) $x = 0$ (*b*) $x = 0.25$ (**c**) $x = 0.5$ (**d**) $x = 0.75$ (**e**) $x = 1.0$

copper in the sample can be ascribed to the smaller volume of Cu^{2+} ions (radius = 0.069 nm) as compared to Zn^{2+} (radius 0.074 nm).

The FTIR spectra consist of two broad bands, one at 580 cm^{-1} which may be assigned to the M-O stretching mode at the tetrahedral site and the other at 400 cm^{-1} may be assigned to the M–O stretching mode at the octahedral site.

Table 1 Particle size and cell size of $Zn_{1-x}Cu_xFe_2O_4$

S. No.	Sample	Particle Size (nm)	Cell size (Å)	Acidity m.moles/g	Surface area m^2/g
1	$ZnFe_2O_4$	18.39	8.473	1.03	32.2
2	$Zn_{075}Cu_{0.25}Fe_2O_4$	10.45	8.457	1.48	50.8
3	$Zn_{0.5}Cu_{0.5}Fe_2O_4$	11.82	8.442	2.35	51.1
4	$Zn_{0.25}Cu_{0.75}Fe_2O_4$	12.49	8.375	2.38	56.1
5	$CuFe_2O_4$	13.99	8.340	3.2	58.4

The Mössbauer spectra of most representative zinc-copper ferrites are reproduced in Fig. 2. On the basis of the spectral shape, this ferrite system can be divided into two categories namely I—Zinc rich ferrite and II—Copper rich ferrite. In Category I i.e. $ZnFe_2O_4$ the spectrum is a single doublet without any sextet indicating the absence of magnetic hyperfine field. This is expected, as zinc is a nonmagnetic element. Bulk $ZnFe_2O_4$ also shows a doublet, which is attributed to its paramagnetic behaviour. The doublet in the present sample of $ZnFe_2O_4$ seems to be due to superparamagnetism exhibited by nanosize particles. The superparamagnetism in $ZnFe_2O_4$ is possible due to the exchange of sites by Zn^{2+} and Fe^{2+} and the resulting A–B superexchange interaction [2, 17]. This view is supported by the magnetic studies as well (Banarjee, in preparation).

The bridge to category II is through $Zn_{0.5}Cu_{0.5}Fe_2O_4$ with equal amount of Zn and Cu atoms. Although the sextet in this spectrum is not clear the spectrum seems to be a superposition of a doublet and a sextet. The doublet and sextet areas can be ascribed to the population of small and large size particles respectively.

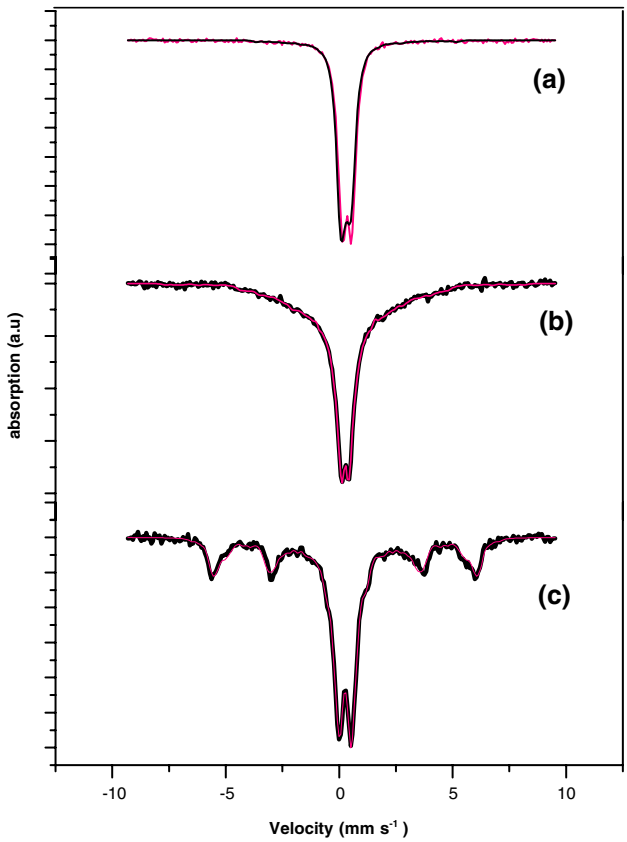

Fig. 2 Mössbauer spectra of $Zn_{1-x}Cu_xFe_2O_4$ (**a**) $x = 0$ (**b**) $x = 0.5$ (**c**) $x = 1.0$

Table 2 Mössbauer parameters of $Zn_{1-x}Cu_xFe_2O_4$

S.No.	Sample	Quadrupole splitting mm s^{-1} (±.005)	Isomer shift mm s^{-1} (±.001)	Area (%)
1	$CuFe_2O_4$	0.66	0.26	58
2	$Zn_{0.5}Cu_{0.5}Fe_2O_4$	0.79	0.28	75
3	$ZnFe_2O_4$	0.48	0.35	100

The large doublet to sextet ratio suggests higher population of small size particles, which leads to superparamagnetic behaviour as supported by magnetic studies (Banarjee, in preparation).

In case of the copper rich $CuFe_2O_4$, the sextet grows still further while the doublet is still present indicating the presence of ferrimagnetic and superparamagnetic particles. The room temperature Mössbauer spectra of bulk $CuFe_2O_4$ consists of a sextet as shown by Evans and Hafner [13] is attributed to the large size particles.

As the doublet is dominant in all the samples, hence only this will be considered for discussing the bonding in these ferrites. The isomer shift (I.S) is an important bonding parameter. IS range (0.26–0.36 mm s^{-1}) in Table 2 suggests the presence of Fe^{3+} iron in these ferrites [18]. The small difference in the isomer shift can be attributed to the difference in the Fe–O bond character in various ferrites. The decrease in the IS values with the increase in the copper content indicates decrease in the s-electron density at the nucleus of the resonant atom and decrease of Fe–O covalency [19]. This is in agreement with the findings of acidity measurements (Table 1).

Low value of quadrupole splitting (Q.S) in case of $ZnFe_2O_4$ (0.48 mm s^{-1}) is typical of Fe^{3+} in octahedral surrounding. The increase in Q.S. to 0.66 mm s^{-1} for $CuFe_2O_4$ seems to be caused by Jahn Teller effect due to copper ions which prefer octahedral site. The Q.S. is maximum (0.79 mm s^{-1}) in case of mixed ferrite i.e. $Zn_{0.5}Cu_{0.5}Fe_2O_4$ which may be attributed to the presence of two different cations instead of one introducing a kind of lattice stress and introduce additional asymmetry.

The asymmetry in the Fig. 2(a–c) can be attributed to transfer of few iron ion from octahedral to tetrahedral sites , maximum being in $CuFe_2O_4$. We can therefore conclude that the octahedral site in $ZnFe_2O_4$ is mostly occupied by Fe^{3+} while in case of $CuFe_2O_4$ the octahedral site is shared by Cu^{2+} and Fe^{3+}. This difference in the cation distribution in different ferrites is the key to their different catalytic behaviour and is discussed later in this section.

The results of BET surface area, acidity are recorded in Table 1, along with the XRD data. A perusal of the data shows that the surface area of $ZnFe_2O_4$ is the lowest 32.2 m^2/g, which is expected, as the particle size of $ZnFe_2O_4$ is the largest. As the copper content is increased, the surface area jumps to 50.8 m^2/g due to the sharp reduction in the particle size. The acidity is proportional to copper content in the samples. The result is similar to that observed in case of zinc-manganese mixed ferrites [9] where acidity increased gradually with manganese content.

The data on the performance of various zinc-copper ferrite catalysts in the methylation of pyridine are presented in Table 3. Inspection of Table 3 indicates that the conversion of pyridine and the yield as well as selectivity for 3-methyl pyridine increase with copper content in the $ZnFe_2O_4$ system with $CuFe_2O_4$ exhibiting the best performance. This trend is directly proportional to the surface area and acidity of various catalysts. Similar trends were found for $Zn_{1-x}Mn_xFe_2O_4$ catalyst [9] for the alkylation of pyridine. It is known that octahedral sites are at the surface of the spinels and are responsible for their catalytic activity. Better performance of $CuFe_2O_4$ compared to $ZnFe_2O_4$ can be attributed to possibility of presence of Cu ions in the octahedral sites as indicated by Mössbauer effect, higher tendency of Cu^{2+} ions towards complexation as compared to Zn^{2+}. The better performance of copper rich catalysts can also be attributed to the decreased particle size, higher surface area and higher number of coordination sites. The mechanism of adsorption seems to be due to the transfer of electrons from pyridine to the vacant

Table 3 Performance of various catalysts in the alkylation of pyridine. Methanol/pyridine molar ratio = 5, temperature = 673 K, WHSV = 0.2 h^{-1}

S.No.	Catalyst	Pyridine conversion (%)	Product distribution (%)		
			Pyridine	2-Methyl Pyridine	3-Methyl Pyridine
1.	$ZnFe_2O_4$	24.00	76.0	22.7	1.3
2.	$Zn_{075}Cu_{0.25}Fe_2O_4$	46.90	53.10	15.7	31.2
3.	$Zn_{0.5}Cu_{0.5}Fe_2O_4$	52.72	47.28	13.2	39.52
4.	$Zn_{0.25}Cu_{0.75}Fe_2O_4$	70.82	29.28	10.8	60.02
5.	$CuFe_2O_4$	92.71	7.29	9.2	83.51

d-orbitals of the transition metals (copper/iron) occupying octahedral site. Introduction of copper in the catalyst system facilitates this process because of which pyridine can form outer d-orbital complex with copper as compared to inner complexes with iron. Since the performance of catalyst is dependent on adsorption, introduction of copper leads to better performance.

Conclusions

$Zn_xCu_{1-x}Fe_2O_4$ nanoparticles were successfully prepared at low temperature by co-precipitation method. XRD pattern shows spinel structure for each sample. Introduction of copper results in reduction in the particle size, reduction in lattice parameter and increase in the surface area. Mössbauer studies suggests (1) decrease in covalency of Fe–O bond due to introduction of copper and (2) occupation of octahedral sites by Cu as well as Fe ions. The methylation of pyridine is found to be highest for $CuFe_2O_4$. The catalytic performance is found to be proportional to surface area and acidity. Higher activity of $CuFe_2O_4$is attributed to the presence of Cu and Fe in octahedral sites as found from Mössbauer measurements.

Acknowledgements The authors wish to express sincere thanks to the UGC-DAE Consortium for Scientific Research (UGC-DAE-CSR), Indore center for recording Mössbauer spectra and XRD pattern of the samples and to Dr. A. Gupta, Center Director UGC-DAE-CSR, Indore center for fruitful discussions and helpful suggestions.

References

1. Mazen SA, Mansour SF, Zaki HM (2003) Crys Res Technol 38:471
2. Chandana Rath N, Mishra C, Anand S, Das RP, Sahu KK, Chandan Upadhyay, Verma HC (2000) Appl Phys Lett 76:475
3. Morrish A, Clark PE (1975) Phys Rev B 11:278
4. Petit A, Forester DW (1971) Phys Rev B 4:3912
5. Jacobs HP, Malitha A, Reintyes JCH, Drimal J, Ponee V, Brogerma HH (1994) J Catal 147:194
6. Toledo JA, Valenzuela A, Bosch P, Amendariz H, Montoya A, Nova N, Vazquez A (2001) Appl Catal A 218:39
7. Kashiwazi H, Fujiki Y, Enomoto S (1982) Chem Pharm Bull 30:2575
8. Kashiwazi H, Enomoto S (1982) Chem Bull 30:404
9. Radheshyam A, Dwivedi R, Reddy VS, Charry KVR, Prasad R (2002) Green Chemistry 4:558
10. Sreekumar K, Mathew T, Devassy BM, Rajgopal R, Vetrivel R, Rao BS (2001) Appl Catal A 205:11
11. Depyrot J, da Silva GJ, Alvert CR, Sousa EC, Magalhäes M, Figueiredo Neto AM, Sousa MH, Tourinho FA (2001) Braz J Phys 31:390
12. ASTM Table No. 22–1012.
13. Evans BJ, Hafner SS (1968) J Phys Chem Solids 29:1573
14. Roy S, Ghose G (2000) J Appl Phys 87:6226
15. ASTM Table No. 25–0283
16. Cullity BD (1956) In: Elements of X-ray diffraction, Addison Wesley publishing company INC, p 99
17. Goya GF, Leite ER (2003) J Phys Condens Matter 15:641
18. Bhide VG (1973) In: Mössbauer effect and its applications, Tata McGraw-Hill Publishing Co.Ltd., New Delhi, p 349
19. Toledo JA, Valenzuela A, Bosch P, Amendariz H, Montoya A, Nova N, Vazquez A (2000) Appl Catal A 198:235